Chapter 1

Alpha Decay: Tunneling and the Gamow Factor

> *"The central feature of this one-body model is that the α particle is preformed inside the parent nucleus... the theory works quite well, especially for even–even nuclei."*
> K. S. Krane [6]

Lecture 16 established the observables Q and $t_{1/2}$, the Geiger–Nuttall correlation, and the nuclear-well plus Coulomb-barrier potential. This chapter derives the Gamow tunneling factor in full: rectangular-barrier warm-up with the *reduced mass* μ, the Coulomb-barrier integral evaluated without skipped steps, the assault frequency, the decay rate $\lambda = S_\alpha\, f\, P$, and the fine structure of α spectra from angular-momentum and parity selection rules [6, 1, 14, 2].

1.1 Classically forbidden region

The available energy $E = Q$ of an emitted α particle is typically 4–9 MeV, much less than the Coulomb barrier height $B \sim 20$–$30\,\mathrm{MeV}$ at the nuclear surface. Three regions of the radial potential are distinguished (Fig. 1.1):

(i) **Well ($r < R$).** The α moves inside the attractive nuclear potential (depth $V_0 \sim 35\,\mathrm{MeV}$) with kinetic energy approximately $Q + V_0$.

(ii) **Barrier ($R < r < b$).** The Coulomb potential exceeds the total energy Q. Classically the particle cannot enter this region: its kinetic energy would have to be negative.

(iii) **Asymptotic ($r > b$).** The Coulomb potential falls below Q; the α escapes with kinetic energy Q.

The outer *classical turning point* b is defined by

$$V_\mathrm{C}(b) = Q, \qquad b = \frac{Z_1 Z_2 e^2}{4\pi\varepsilon_0\, Q}, \tag{1.1}$$

with $Z_1 = Z - 2$ (daughter charge) and $Z_2 = 2$ (α charge).

Quantum mechanics permits a non-zero probability for the α to traverse the classically forbidden interval $R \le r \le b$. Dunlap expresses the lifetime as $\tau = \tau_0/P$, where P is the escape

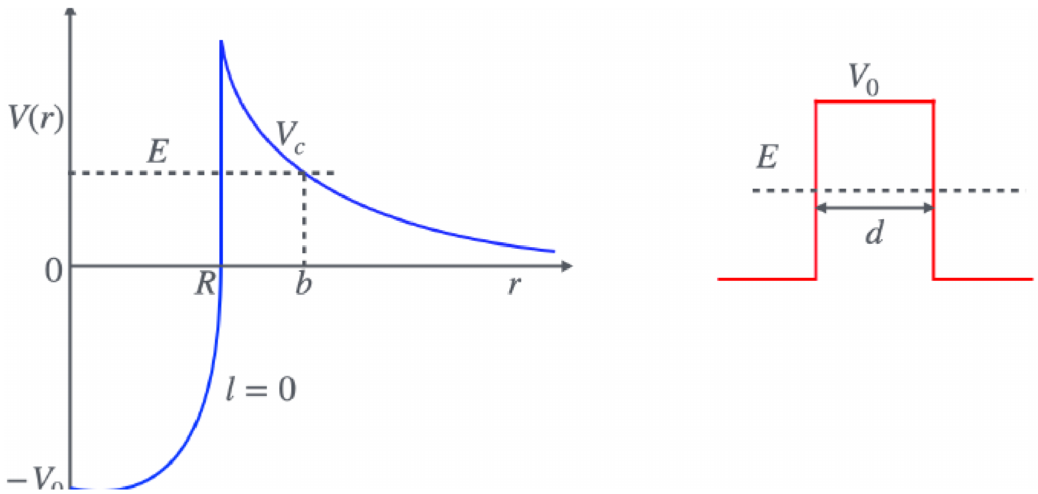

Figure 1.1: Left: nuclear well plus Coulomb barrier with total energy $E = Q$, inner radius R, and outer turning point b. Right: rectangular barrier of height V_0 and width d used as a warm-up for tunneling theory. Re-extracted from the original PH5001 lecture source pages.

probability and τ_0 is a formation time scale; the course uses the equivalent form $\lambda = S_\alpha f P$ with assault frequency f and preformation factor S_α [1, 6].

1.2 Rectangular barrier and the reduced mass

For a one-dimensional rectangular barrier of height $V_0 > E$ and width d, the Schrödinger equation in the forbidden region gives an evanescent wavefunction $\psi \propto e^{-\gamma r}$ with

$$\gamma = \frac{\sqrt{2\mu(V_0 - E)}}{\hbar}, \tag{1.2}$$

where μ is the *reduced mass* of the α-daughter system:

$$\mu = \frac{m_\alpha M_d}{m_\alpha + M_d}. \tag{1.3}$$

For heavy nuclei $M_d \gg m_\alpha$, so $\mu \approx m_\alpha$ to good approximation, but all barrier formulas must be written with μ for consistency with the two-body Coulomb problem [1].

Matching the wavefunction and its derivative at the barrier boundaries yields the standard WKB result for the transmission probability:

$$P \approx e^{-2\gamma d} = \exp\left[-\frac{2d}{\hbar}\sqrt{2\mu(V_0 - E)}\right]. \tag{1.4}$$

The factor $(V_0 - E)$ is the amount by which the potential exceeds the particle energy inside the barrier.

1.3 Coulomb barrier and the Gamow integral

For a non-rectangular barrier, one divides the interval into slices of width $\mathrm{d}r$ and multiplies the elementary penetration factors. This WKB approximation gives

$$P \approx \exp\left[-2\int_R^b \gamma(r)\,\mathrm{d}r\right] = e^{-2G}, \tag{1.5}$$

where

$$\gamma(r) = \frac{\sqrt{2\mu[V(r)-Q]}}{\hbar}, \qquad G = \int_R^b \gamma(r)\,\mathrm{d}r. \tag{1.6}$$

Barrier excess measured from the turning point. For $R \le r \le b$, the quantity that enters the WKB wave number is

$$V_{\mathrm{C}}(r) - Q = \frac{Z_1 Z_2 e^2}{4\pi\varepsilon_0}\left(\frac{1}{r} - \frac{1}{b}\right), \tag{1.7}$$

which vanishes at b, since $Q = Z_1 Z_2 e^2/(4\pi\varepsilon_0 b)$. Substituting into Eq. (1.39):

$$G = \frac{\sqrt{2\mu}}{\hbar}\sqrt{\frac{Z_1 Z_2 e^2}{4\pi\varepsilon_0}}\int_R^b \sqrt{\frac{1}{r} - \frac{1}{b}}\,\mathrm{d}r. \tag{1.8}$$

1.4 Evaluating the integral: every step

Define

$$I = \int_R^b \sqrt{\frac{1}{r} - \frac{1}{b}}\,\mathrm{d}r = \int_R^b \sqrt{\frac{b-r}{br}}\,\mathrm{d}r. \tag{1.9}$$

Step 1: Trigonometric substitution. Set

$$r = b\sin^2\theta. \tag{1.10}$$

Differentiate:

$$\mathrm{d}r = 2b\sin\theta\cos\theta\,\mathrm{d}\theta. \tag{1.11}$$

Express $1/r$:

$$\frac{1}{r} = \frac{1}{b\sin^2\theta}. \tag{1.12}$$

Form the combination under the square root:

$$\frac{1}{r} - \frac{1}{b} = \frac{1}{b\sin^2\theta} - \frac{1}{b} = \frac{1-\sin^2\theta}{b\sin^2\theta} = \frac{\cos^2\theta}{b\sin^2\theta}. \tag{1.13}$$

Take the square root (positive in the interval of interest):

$$\sqrt{\frac{1}{r} - \frac{1}{b}} = \sqrt{\frac{\cos^2\theta}{b\sin^2\theta}} = \frac{\cos\theta}{\sqrt{b}\,\sin\theta} = \frac{\cot\theta}{\sqrt{b}}. \tag{1.14}$$

Step 2: Rewrite the integral in θ.

$$I = \int \frac{\cot\theta}{\sqrt{b}} \cdot 2b \sin\theta\cos\theta\,\mathrm{d}\theta. \tag{1.15}$$

Simplify the integrand:

$$\frac{\cot\theta}{\sqrt{b}} \cdot 2b\sin\theta\cos\theta = \frac{\cos\theta}{\sin\theta\sqrt{b}} \cdot 2b\sin\theta\cos\theta = \frac{2b\cos^2\theta}{\sqrt{b}} = 2\sqrt{b}\cos^2\theta. \tag{1.16}$$

Hence

$$I = 2\sqrt{b}\int \cos^2\theta\,\mathrm{d}\theta. \tag{1.17}$$

Step 3: Integrate $\cos^2\theta$. Use $\cos^2\theta = \frac{1}{2}(1+\cos 2\theta)$:

$$I = 2\sqrt{b}\int \frac{1+\cos 2\theta}{2}\,\mathrm{d}\theta = \sqrt{b}\int (1+\cos 2\theta)\,\mathrm{d}\theta = \sqrt{b}\left(\theta + \frac{\sin 2\theta}{2}\right). \tag{1.18}$$

Step 4: Limits of integration. When $r = R$:

$$\sin^2\theta_R = \frac{R}{b} \quad \Rightarrow \quad \theta_R = \arcsin\sqrt{\frac{R}{b}}. \tag{1.19}$$

When $r = b$:

$$\sin^2\theta_b = 1 \quad \Rightarrow \quad \theta_b = \frac{\pi}{2}. \tag{1.20}$$

Step 5: Evaluate at the limits.

$$I = \sqrt{b}\left[\frac{\pi}{2} + \frac{\sin\pi}{2}\right] - \sqrt{b}\left[\arcsin\sqrt{\frac{R}{b}} + \frac{\sin(2\theta_R)}{2}\right]. \tag{1.21}$$

Since $\sin\pi = 0$:

$$I = \sqrt{b}\left[\frac{\pi}{2} - \arcsin\sqrt{\frac{R}{b}} - \frac{\sin(2\theta_R)}{2}\right]. \tag{1.22}$$

Step 6: Simplify $\sin(2\theta_R)$. Use $\sin(2\theta_R) = 2\sin\theta_R\cos\theta_R$ with $\sin\theta_R = \sqrt{R/b}$ and $\cos\theta_R = \sqrt{1-R/b}$:

$$\sin(2\theta_R) = 2\sqrt{\frac{R}{b}}\sqrt{1-\frac{R}{b}} = 2\sqrt{\frac{R}{b}\left(1-\frac{R}{b}\right)}. \tag{1.23}$$

Therefore

$$\frac{\sin(2\theta_R)}{2} = \sqrt{\frac{R}{b}\left(1-\frac{R}{b}\right)}. \tag{1.24}$$

Step 7: Use arccos form. Since $\arccos x + \arcsin x = \pi/2$,

$$\frac{\pi}{2} - \arcsin\sqrt{\frac{R}{b}} = \arccos\sqrt{\frac{R}{b}}. \tag{1.25}$$

The final result is

$$I = \sqrt{b}\left[\arccos\sqrt{\frac{R}{b}} - \sqrt{\frac{R}{b}\left(1-\frac{R}{b}\right)}\right]. \tag{1.26}$$

Step 8: Assemble G and P. Substituting Eq. (1.26) into Eq. (1.8):

$$G = \frac{b}{\hbar}\sqrt{2\mu Q}\left[\arccos\sqrt{\frac{R}{b}} - \sqrt{\frac{R}{b}\left(1-\frac{R}{b}\right)}\right], \tag{1.27}$$

where we used $Q = Z_1Z_2e^2/(4\pi\varepsilon_0 b)$, so the two factors of $\sqrt{b}$ combine to b. This form is dimensionless; an extra $\sqrt{b}$ would make G dimensionful. The tunneling probability is

$$P = e^{-2G}. \tag{1.28}$$

1.5 Barrier height B and the small Q/B limit

The Coulomb barrier height at $r = R$ is

$$B = \frac{Z_1Z_2e^2}{4\pi\varepsilon_0\, R}, \qquad \frac{R}{b} = \frac{Q}{B}. \tag{1.29}$$

In terms of B and Q, Eq. (1.27) becomes

$$G = \frac{Z_1Z_2e^2}{4\pi\varepsilon_0\,\hbar}\sqrt{\frac{2\mu}{Q}}\left[\arccos\sqrt{\frac{Q}{B}} - \sqrt{\frac{Q}{B}\left(1-\frac{Q}{B}\right)}\right]. \tag{1.30}$$

Small Q/B expansion. For typical α decays, $Q/B \sim 0.1$–0.2. Expand for $Q/B \ll 1$:

$$\arccos\sqrt{\frac{Q}{B}} \approx \frac{\pi}{2} - \sqrt{\frac{Q}{B}}, \qquad \sqrt{\frac{Q}{B}\left(1-\frac{Q}{B}\right)} \approx \sqrt{\frac{Q}{B}}. \tag{1.31}$$

The bracket becomes $\pi/2 - 2\sqrt{Q/B}$. Keeping the leading term $\pi/2$ and using $Q = \frac{1}{2}\mu v^2$ for the asymptotic α speed v:

$$G \approx \frac{\pi Z_1Z_2e^2}{4\pi\varepsilon_0\,\hbar v} = \frac{Z_1Z_2e^2}{4\varepsilon_0\,\hbar v}, \qquad v = \sqrt{\frac{2Q}{\mu}}. \tag{1.32}$$

Thus $P \sim \exp(-2G)$ depends exponentially on $1/v \propto Q^{-1/2}$, which is the Geiger–Nuttall rule [6, 1, 14].

Key idea

Because $P \sim \exp(-c/\sqrt{Q})$, a small increase in Q reduces G and multiplies the decay rate by many orders of magnitude. The Geiger–Nuttall rule is a direct consequence of Coulomb-barrier tunneling.

1.6 Assault frequency, preformation, and $\lambda = S_\alpha f P$

The tunneling probability P is the escape probability *per attempt*. The α bounces inside the well, presenting itself at the barrier with characteristic frequency f. The decay constant is

$$\lambda = S_\alpha\, f\, P, \tag{1.33}$$

where S_α is the *preformation factor* (probability that nucleons are clustered as an α at the barrier surface). It is a model-dependent overlap factor, not a universal observable; setting $S_\alpha = 1$ is only a crude single-particle upper-normalisation. Extracted values depend on the barrier radius and nuclear-structure model, and hindered transitions can have $S_\alpha \ll 1$ [6].

Assault frequency. If the α travels back and forth across diameter $2R$ at interior speed v_0, the time for one round trip is $2R/v_0$, so

$$f = \frac{v_0}{2R}. \tag{1.34}$$

Inside the well the kinetic energy is $Q + V_0$ (where V_0 is the well depth, typically $\sim 35\,\text{MeV}$):

$$\frac{1}{2}\mu v_0^2 = Q + V_0 \quad \Rightarrow \quad v_0 = \sqrt{\frac{2(Q+V_0)}{\mu}}. \tag{1.35}$$

Hence

$$f = \frac{1}{2R}\sqrt{\frac{2(Q+V_0)}{\mu}} = \sqrt{\frac{Q+V_0}{2\mu R^2}}. \tag{1.36}$$

Combining with Eq. (1.28):

$$\lambda = S_\alpha \sqrt{\frac{Q+V_0}{2\mu R^2}}\, e^{-2G}, \qquad t_{1/2} = \frac{\ln 2}{\lambda}. \tag{1.37}$$

Caution

Absolute half-life calculations are extremely sensitive to the assumed radius: Krane notes that a 4% change in R can change calculated $t_{1/2}$ by a factor of about five. Measured lifetimes are therefore sometimes used to infer an effective sum of nuclear and α radii [6].

1.7 Fine structure, branching, and selection rules

When the daughter is left in an excited state, each branch has its own $Q_i = Q_{\text{gs}} - E_i^*$ and its own required orbital angular momentum ℓ carried by the α. The centrifugal barrier adds $\hbar^2\ell(\ell+1)/(2\mu r^2)$ to $V(r)$, raising G and suppressing high-ℓ branches [6, 1].

Selection rules. The α particle has $J^\pi = 0^+$: intrinsic spin 0 and positive intrinsic parity. Angular momentum and parity conservation therefore require

$$\boldsymbol{J}_i = \boldsymbol{J}_f + \boldsymbol{\ell}, \qquad \pi_i = \pi_f \times (-1)^\ell. \tag{1.38}$$

Allowed ℓ values satisfy $|J_i - J_f| \le \ell \le J_i + J_f$ with the parity condition. In practice, the lowest allowed ℓ dominates because it minimises the barrier.

1.7.1 Even–even example: $^{244}\text{Cm} \to {}^{240}\text{Pu}$

Both parent and daughter ground states are 0^+. The daughter rotational band begins at 2^+ (42.824 keV), 4^+ (141.690 keV), and 6^+ (294.319 keV) [20, 21]. DDEP/LNHB evaluated absolute α-emission probabilities are [20, 21, 28]:

Daughter state	E^* (keV)	ℓ	Branch (%)
0^+ (gs)	0	0	76.7(4)
2^+	42.824	2	23.3(4)
4^+	141.690	4	0.0204(15)
6^+	294.319	6	0.00352(18)

The ground-state branch ($\ell = 0$) dominates. The 2^+ branch has both a smaller Q_i and an $\ell = 2$ centrifugal barrier. Higher members of the rotational band are strongly suppressed; note especially that the 4^+ and 6^+ probabilities are hundredths and thousandths of a percent, respectively [6, 28].

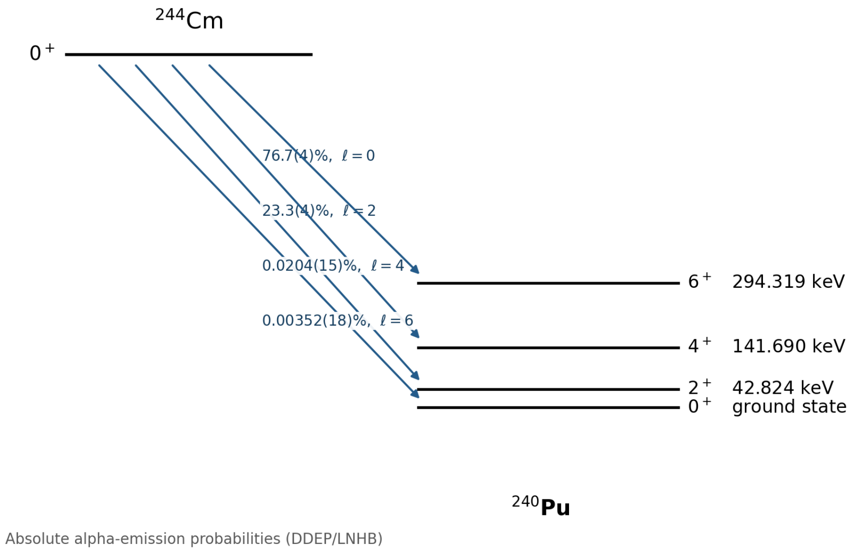

Figure 1.2: Branching ratios for α decay of ^{244}Cm to levels of ^{240}Pu. Original decay-scheme redraw for these notes using DDEP/LNHB evaluated absolute α-emission probabilities [20, 21, 28]; source URLs are recorded in `figures/lecture17/SOURCES.txt`.

1.7.2 Odd-A example: $^{243}\text{Am} \to {}^{239}\text{Np}$

Remark

The original lecture slides incorrectly labelled this case as ^{249}Am. The correct parent is ^{243}Am ($J^\pi = \frac{5}{2}^-$), which α-decays to ^{239}Np ($J^\pi = \frac{5}{2}^+$ ground state) [20, 21, 6].

Ground-state branch. Parent $\frac{5}{2}^-$ to daughter $\frac{5}{2}^+$ requires a change of parity, so ℓ must be odd. The lowest allowed value is $\ell = 1$. The centrifugal barrier makes this branch highly hindered: evaluated data give a branching ratio of only 0.240(3)% [20, 21, 28].

Dominant branch to $\frac{5}{2}^-$ at 74.660 keV. The daughter level at $E^* = 74.660\,\text{keV}$ has $J^\pi = \frac{5}{2}^-$, matching the parent parity. An $\ell = 0$ transition is therefore allowed. Although Q_i is reduced, the much thinner $\ell = 0$ barrier dominates, and this branch carries 86.74(5)% of the α intensity [20, 21, 28, 6].

Other branches. The 31.130 keV, $\frac{7}{2}^+$ level receives 0.192(3)% and requires odd ℓ, with $\ell_{\min} = 1$. The 117.84 keV, $\frac{7}{2}^-$ and 173.02 keV, $\frac{9}{2}^-$ levels receive 11.46(5)% and 1.383(7)%, respectively; parity is unchanged and $\ell_{\min} = 2$ for both. Figure 1.3 shows these principal DDEP branches.

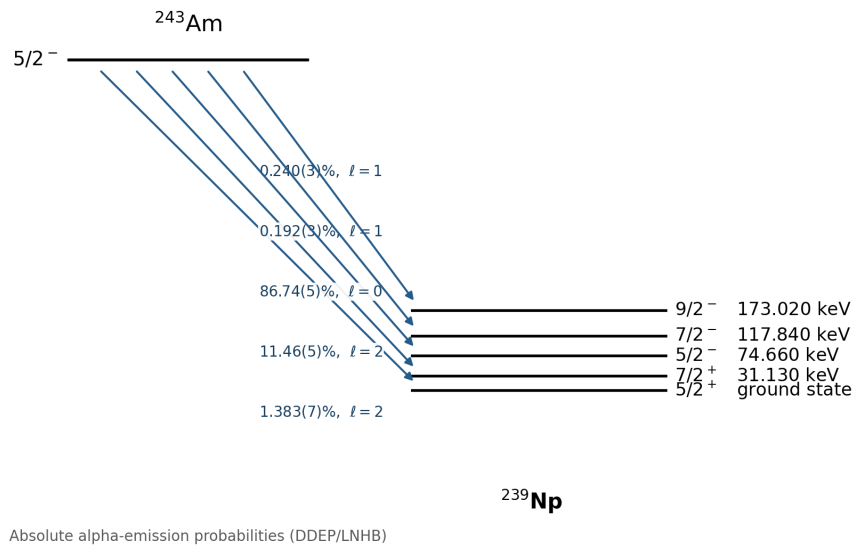

Figure 1.3: Branching ratios for α decay of ^{243}Am to levels of ^{239}Np. Original decay-scheme redraw for these notes using DDEP evaluated absolute α-emission probabilities; the isotope is corrected from ^{249}Am to ^{243}Am [20, 21, 28]. Source URL: `figures/lecture17/SOURCES.txt`.

Hindrance factors. The hindrance factor $F = \lambda_{\text{theory}}/\lambda_{\text{exp}}$ (or equivalently the ratio of predicted to observed branch intensity) quantifies deviations from the Gamow estimate. Large F indicates poor parent-daughter overlap or selection-rule suppression beyond the centrifugal barrier [6].

1.8 Why many nuclei with $Q > 0$ still appear stable

The SEMF gives $Q_\alpha > 0$ already near $A \sim 150$, yet many nuclides up to ^{208}Pb are stable or long-lived. If G is large, e^{-2G} is extraordinarily small and $t_{1/2}$ can exceed 10^{17} s ($\sim 10^{10}$ years). Only when Q rises into the actinide range do laboratory half-lives become short. This is precisely the Geiger–Nuttall message encoded in $P = e^{-2G}$: $Q > 0$ is necessary for spontaneous α decay, but the half-life is fixed by tunneling.

Takeaway

The Gamow theory explains (i) why $Q > 0$ does not imply short lifetimes, (ii) the Geiger–Nuttall $Q^{-1/2}$ correlation, and (iii) the fine structure of α spectra through ℓ-dependent barriers and selection rules. Use reduced mass μ throughout, and remember $\lambda = S_\alpha f P$.

1.9 Deeper physics: the Gamow factor and WKB tunneling

1.9.1 The Gamow integral for a Coulomb barrier

For $\ell = 0$ and energy $E = Q$, the WKB penetration exponent for a Coulomb barrier is the Gamow integral

$$G = \int_R^b \kappa(r)\,\mathrm{d}r, \qquad \kappa(r) = \frac{\sqrt{2\mu[V_\mathrm{C}(r) - Q]}}{\hbar}, \tag{1.39}$$

with inner radius R and outer turning point $b = Z_1 Z_2 e^2/(4\pi\varepsilon_0 Q)$ from (1.1) [6, 1]. Evaluating the integral for a pure Coulomb tail gives the standard form

$$G \approx \frac{Z_1 Z_2 e^2}{4\pi\varepsilon_0\hbar}\sqrt{\frac{2\mu}{Q}}\left[\arccos\sqrt{\frac{Q}{V_\mathrm{C}(R)}} - \sqrt{\frac{Q}{V_\mathrm{C}(R)}\left(1 - \frac{Q}{V_\mathrm{C}(R)}\right)}\right], \tag{1.40}$$

and the escape probability is $P \approx e^{-2G}$. The reduced mass $\mu = m_\alpha M_d/(m_\alpha + M_d)$ enters every WKB formula; for heavy parents $\mu \simeq m_\alpha$ to within a few percent [1].

Order-of-magnitude Gamow exponent

For ^{212}Po ($Z = 84$, $Q \approx 8.95\,\mathrm{MeV}$), take $R \approx 1.2\,A^{1/3}\,\mathrm{fm} \approx 7\,\mathrm{fm}$ and $V_\mathrm{C}(R) \approx 25\,\mathrm{MeV}$. Then $2G \sim 30$–40, so $P \sim e^{-2G} \sim 10^{-14}$ and, with an assault frequency $f \sim 10^{21}\,\mathrm{s}^{-1}$, $\lambda \sim 10^7\,\mathrm{s}^{-1}$, consistent with the microsecond half-life [6, 14]. A 4% increase in effective R lengthens $t_{1/2}$ by roughly a factor of five because G is so steep [6].

1.9.2 Rectangular barrier as a WKB warm-up

Before the Coulomb integral, a rectangular barrier of height $V_0 > E$ and width d gives (1.4). The exponent is linear in d and in $\sqrt{V_0 - E}$, with μ in the denominator of γ. This model captures the essential physics: classically forbidden regions admit exponentially small transmission, and heavier ejectiles (larger μ) or lower Q (thicker barrier) suppress the rate dramatically. The full Gamow result replaces the constant height by the $1/r$ Coulomb tail, which is why $\log t_{1/2}$ tracks $Q^{-1/2}$ rather than a simple exponential in Q [25, 2].

Key idea

Assault frequency and preformation. The decay rate is $\lambda = S_\alpha\, f\, P$ with preformation factor S_α and assault frequency $f \sim v/(2R)$. Gamow theory explains the Q dependence through $P = e^{-2G}$; shell effects and hindrance enter S_α. Even–even nuclei with $F \approx 1$ validate the minimal model; large hindrance factors signal poor cluster overlap at the surface [6, 14].

1.9.3 Centrifugal barrier and angular momentum

For $\ell \neq 0$ the effective barrier acquires a centrifugal term $\hbar^2\ell(\ell+1)/(2\mu r^2)$ that raises G and lengthens $t_{1/2}$. Fine-structure α groups populating excited daughter states with spin $I > 0$ therefore require a larger Gamow exponent than ground-state $\ell = 0$ decay [6, 1]. In fusion, the same centrifugal term suppresses low-energy cross sections for partial waves with $\ell > 0$, filtering which angular-momentum channels contribute at sub-barrier energies (Lecture 25) [14]. The rectangular-barrier warm-up (1.4) is the constant-height limit; the Coulomb tail makes G depend on $\log Q$ as well as $1/\sqrt{Q}$, which is why the Geiger–Nuttall slope is not a simple exponential in Q alone.

1.9.4 Deformed nuclei and effective barrier radii

For deformed heavy nuclei ($A \gtrsim 230$) the Coulomb barrier is not spherically symmetric at the surface. The α cluster exits preferentially where the barrier is lowest, effectively reducing the barrier width compared with a spherical average [6, 1]. Practitioners sometimes quote an *effective* radius R_{eff} fitted to measured half-lives; a 4% change in R_{eff} can shift $t_{1/2}$ by about a factor of five because of the exponential in G [6]. This sensitivity is the same reason that sub-barrier fusion cross sections (Lecture 25) are difficult to predict from a single contact radius: orientation and deformation matter as much as the spherical estimate [53]. Fine-structure studies that compare ground-state and excited-state α branches constrain both R_{eff} and the hindrance factor S_α [14].

Key idea

Exponential leverage. If $2G \sim 60$, then $\Delta G = 1$ changes P by a factor $e^2 \sim 7$. Barrier modeling at the mega-electronvolt level is therefore mandatory for order-of-magnitude half-lives, which is why Lecture 16's Geiger–Nuttall correlation is powerful yet not a substitute for a full WKB evaluation when Q or Z changes substantially.

1.10 Further physics from the literature

Radius sensitivity and effective sizes. Absolute Gamow half-lives depend exponentially on R through both G and f. Krane reports that a 4% change in the radius parameter can shift calculated $t_{1/2}$ by a factor of about five; practitioners sometimes invert the problem and infer an effective R-sum from measured lifetimes [6]. Deformed nuclei ($A \gtrsim 230$) further modify the barrier because the Coulomb potential is not spherically symmetric at the surface.

Preformation and cluster decay. The preformation factor S_α accounts for the probability that four nucleons are correlated as an α at the nuclear surface. Heavier cluster emissions (^{14}C, ^{24}Ne, and others) use the same $P = e^{-2G}$ framework but with larger reduced mass, higher Coulomb barrier, and vastly smaller S_α [6, 1, 14]. The first observed ^{14}C branch from ^{223}Ra had relative intensity $\sim 10^{-9}$ compared with α decay.

Proton radioactivity. Near the proton drip line, one-proton emission becomes the $Z_2 = 1$ analogue of Gamow theory when $Q_p > 0$. The same WKB integral applies with $Z_1 = Z - 1$, $Z_2 = 1$, and μ replaced by the proton-daughter reduced mass [6, 1].

Alignment experiments. When neither parent nor daughter has spin 0, several ℓ values may contribute to the same transition. Measuring the angular distribution of α particles relative to a spin-aligned source disentangles the ℓ-components; Krane Fig. 8.8 shows such an analysis for aligned ^{253}Es [6].

Reading guide

Krane [6] Sects. 8.4–8.6 (Gamow factor, fine structure, hindrance); Dunlap [1] Sect. 8.2 (WKB derivation with μ); Demtröder [2] Sect. 3.3 (historical context and Gamow peak notation); Basdevant [14] Sect. 2.6 (model and half-life systematics).

1.10.1 Time-reversed Gamow factor and fusion (Lectures 25–26)

Alpha decay and fusion differ only in boundary conditions on the same Coulomb barrier. Outgoing α particles tunnel from $r = R$ to $r = b$; incoming projectiles tunnel inward. The WKB exponent (1.39) is identical in form, with μ now the reduced mass of the colliding pair. For $^{12}\mathrm{C} + ^{12}\mathrm{C}$ at $E_{\mathrm{CM}} = 1\,\mathrm{MeV}$, $2G$ is still large ($\sim$ 15–20), so the fusion cross section remains tiny despite $E > 0$ [6, 14]. Stellar rates average this tunneling probability over a Maxwell–Boltzmann distribution (Lecture 26).

Reduced mass in α decay versus $p + p$ fusion

For ^{212}Po α decay, $\mu \approx m_\alpha$ to 0.5%. For $p + p$ fusion, $\mu = m_p/2$. The Gamow energy parameter $E_G = 2\mu(\pi\alpha\hbar c)^2$ for $p + p$ is orders of magnitude smaller than for heavy-ion fusion because $Z_1Z_2 = 1$. That is why hydrogen burning proceeds at keV Gamow-peak energies while superheavy synthesis requires MeV bombarding energies [36, 53].

1.10.2 From cluster decay to reaction cross sections

Cluster radioactivity generalises Gamow theory: the ejectile carries larger μ and higher Z_1Z_2, so G grows and lifetimes stretch to 10^9 y or more for ^{14}C branches [6, 14]. The same penetration integral appears in heavy-ion fusion when the compound nucleus decays by α emission after capture. Direct-reaction stripping (Lecture 21) probes surface overlap that preformation factors encode in decay; compound-nucleus evaporation (Lecture 22) is the inelastic counterpart of sequential α and γ cascades [6, 37].

Fine-structure α decay to excited daughter states splits one Geiger–Nuttall point into several branches with different Q values. Each branch tests a different radial overlap because the daughter wave function must match a specific final-state configuration. Hindrance factors for odd-A parents play the same role as suppressed spectroscopic factors in transfer reactions: the barrier integral is unchanged, but the nuclear overlap is small [6, 1]. Proton radioactivity near the drip line is the $Z_2 = 1$ limit of the same WKB framework.

Remark

The assault frequency $f \sim v/(2R) \sim 10^{21}\,\mathrm{s}^{-1}$ sets the attempt rate but not the steep Q dependence: changing f by an order of magnitude shifts $\log t_{1/2}$ by only one unit, whereas a modest Q change moves $\log t_{1/2}$ by ten or more. This hierarchy justifies treating G as the primary variable when reading Geiger–Nuttall data, and treating S_α as a secondary correction except for strongly hindered transitions [6, 14].

1.10.3 Cluster decay as a test of the Gamow framework

The first observed ^{14}C branch from ^{223}Ra had relative intensity $\sim 10^{-9}$ compared with α decay [6, 14]. The larger ejectile mass and higher Coulomb charge raise G so much that the preformation factor must also be tiny. Cluster decay is therefore a sensitive probe of both barrier penetration and surface clustering. In the reaction context, light-ion transfer and knockout reactions on radioactive beams test similar overlap integrals at the nuclear surface (Lecture 21) [51]. The course arc from Geiger–Nuttall (Lecture 16) through G (Lecture 17) to sub-barrier fusion (Lecture 25) is one continuous story about exponential sensitivity to barrier geometry.

1.11 Deeper reading: WKB sensitivity and assault frequency

Because $P \sim e^{-2G}$, a 1 MeV shift in barrier height or a change in the inner radius of a few tenths of a femtometre can move half-lives by orders of magnitude. That exponential sensitivity is why microscopic fission theory invests so much effort in inertias and potential-energy surfaces (Lecture 23), not only in a one-dimensional Coulomb integral.

The assault frequency ν in $\lambda = \nu P$ is only an order-of-magnitude prefactor in the pedagogical model; modern calculations replace it with collective inertia along a fission or cluster path. Reduced-mass corrections $\mu \approx m_\alpha(A-4)/A$ matter at the few-percent level for light emitters and less for heavy ones, but they should be written explicitly when comparing textbook estimates to data.

Rectangular versus Coulomb barriers

A rectangular barrier of height V_0 and width L yields $G \approx L\sqrt{2\mu(V_0 - E)}/\hbar$, exposing exponential dependence algebraically. Replacing it with a Coulomb integral changes the Q-dependence into the Geiger–Nuttall form but preserves the exponential message. Students should evaluate both once.

Angular momentum barriers

Emitting α particles with $\ell > 0$ adds a centrifugal term that increases G and suppresses high-ℓ branches. That is why ground-state to ground-state $\ell = 0$ transitions often dominate when spin allows, connecting to selection themes in Lecture 20.

WKB numerical sketch

Approximate a Coulomb barrier as a triangle or use the analytic Gamow integral for ^{212}Po with $Q_\alpha \approx 8.95\,\mathrm{MeV}$. Show that $2G$ is tens of units, so e^{-2G} is astronomically small, yet multiplied by a nuclear assault frequency $\sim 10^{20}\,\mathrm{s}^{-1}$ it can yield a macroscopic half-life. Change Q by $0.5\,\mathrm{MeV}$ and recompute to feel the exponential lever arm.

Relate this sensitivity to fission (Lecture 23): replacing the α Coulomb barrier with a many-dimensional fission barrier preserves the exponential, not the detailed prefactor. Students who master one WKB estimate here will not be surprised by order-of-magnitude fission lifetime uncertainties later.

WKB tunneling is the quantitative engine behind α lifetimes and a prototype for fission and fusion barrier penetration in later lectures.

In practice, rework one numerical estimate from the lecture with a different parameter set and compare the shift to the quoted experimental uncertainty. If the shift exceeds the uncertainty, the estimate is teaching a scale, not delivering a fit. That distinction keeps theoretical cartoons honest when they sit beside evaluated data tables and modern many-body calculations. Along the course arc, write one sentence linking this chapter backward and one forward: the discipline of those two sentences is as important as any single formula. Examination problems rarely ask for a literature review, but they do ask for the scale argument that literature reviews presuppose.

Synthesis problem

Write a half-page note that (i) restates the chapter's central scale or selection rule in one equation, (ii) evaluates it numerically for one concrete nucleus or energy, and (iii) names the neighbouring lecture that uses the result. Keep the note free of research-frontier speculation; the goal is fluency with the lecture physics itself. If an assumption fails (Born approximation, spherical mean field, allowed transition, one-dimensional barrier), state the failure mode in a final sentence. That habit converts passive reading into examination-ready understanding and makes the later research-frontier box read as an extension rather than a replacement.

Research frontier: microscopic tunneling and student projects

The Gamow tunneling picture of Lecture 17 (WKB barrier penetration for α emission) is the conceptual ancestor of modern fission and cluster decay calculations. Today's theory evaluates multidimensional potential-energy surfaces with collective inertias, rather than a one-dimensional Coulomb barrier with an ad hoc assault frequency [54, 53]. Preformation is reframed as the overlap of the parent ground state with a cluster-plus-daughter configuration. Gamow's original insight (exponential sensitivity to the barrier integral) survives, but quantitative half-lives demand controlled many-body input [25]. Remaining uncertainties of even $1\,\mathrm{MeV}$ in barrier height can change spontaneous-fission or cluster-decay lifetimes by orders of magnitude, which is why microscopic inertia and dissipation modelling is as important as the barrier shape itself. The lecture's rectangular-barrier toy model remains the right first step for seeing that exponential dependence analytically.

In fission, the analogue of the assault frequency is a collective inertia along the fission path; different microscopic prescriptions can change lifetimes dramatically even when barriers look similar. Student reading should therefore separate barrier-height uncertainty from inertia uncertainty when comparing published spontaneous-fission half-lives.
Separating barrier-height errors from inertia errors is the practical checklist when comparing published spontaneous-fission half-lives.
Those two error sources rarely scale the same way with mass number, which students can illustrate with a simple WKB model.
Student directions. (1) Analytic estimate: evaluate a rectangular-barrier Gamow factor and show the exponential dependence on width and height. (2) Kinematics check: compare reduced-mass corrections $\mu \approx m_\alpha(A-4)/A$ for $A = 50$ and $A = 250$. (3) Literature reading: from a modern fission-theory review, list two sources of order-of-magnitude uncertainty in WKB half-lives [54].

1.12 Problems with solutions

Problem 17.1 — Turning point b

For α decay with $Z_1 = 90$, $Z_2 = 2$, and $Q = 5.0\,\mathrm{MeV}$, calculate the classical turning point b. Use $e^2/(4\pi\varepsilon_0) = 1.44\,\mathrm{MeV\,fm}$.

Solution 17.1

Step 1. From Eq. (1.1):

$$b = \frac{Z_1 Z_2 e^2/(4\pi\varepsilon_0)}{Q}.$$

Step 2. Numerator:

$$Z_1 Z_2 \times \frac{e^2}{4\pi\varepsilon_0} = 90 \times 2 \times 1.44\,\mathrm{MeV\,fm} = 259.2\,\mathrm{MeV\,fm}.$$

Step 3.

$$b = \frac{259.2\,\mathrm{MeV\,fm}}{5.0\,\mathrm{MeV}} = 51.8\,\mathrm{fm} \approx 52\,\mathrm{fm}.$$

The α is classically forbidden for $R \lesssim r \lesssim 52\,\mathrm{fm}$ [1, 6].

Problem 17.2 — Reduced mass and γ

For α decay of a heavy nucleus ($A = 220$), compute μ in u and estimate γ for a rectangular barrier with $V_0 - E = 20\,\mathrm{MeV}$ and $\hbar c = 197\,\mathrm{MeV\,fm}$.

Solution 17.2

Step 1 (masses). $m_\alpha \approx 4\,\mathrm{u}$, $M_d \approx 216\,\mathrm{u}$.

Step 2 (reduced mass).

$$\mu = \frac{m_\alpha M_d}{m_\alpha + M_d} = \frac{4 \times 216}{220}\,\mathrm{u} = 3.927\,\mathrm{u}.$$

Since $M_d \gg m_\alpha$, μ is close to m_α.

Step 3 (convert to energy units). $1\,\mathrm{u}\,c^2 = 931.5\,\mathrm{MeV}$, so $\mu c^2 = 3.927 \times 931.5 \approx 3658\,\mathrm{MeV}$.

Step 4 (γ).

$$\gamma = \frac{\sqrt{2\mu(V_0 - E)}}{\hbar} = \frac{\sqrt{2 \times 3658 \times 20}}{197\,\mathrm{MeV\,fm}} = \frac{\sqrt{146320}}{197} \approx 1.94\,\mathrm{fm}^{-1}.$$

For a 10 fm wide rectangular barrier, $P \approx e^{-2\gamma d} \approx e^{-38.8} \approx 10^{-17}$ [1].

Problem 17.3 — Gamow factor sensitivity

If $2G = 60$ at one Q and a small increase in Q reduces $2G$ by 5% (from 60 to 57), by what factor does $P = e^{-2G}$ increase? What is the corresponding change in half-life?

Solution 17.3

Step 1 (probability ratio).

$$\frac{P'}{P} = \frac{e^{-57}}{e^{-60}} = e^{3} = 20.1.$$

Step 2 (half-life ratio). Since $t_{1/2} \propto 1/P$:

$$\frac{t'_{1/2}}{t_{1/2}} = \frac{P}{P'} = e^{-3} = 0.050.$$

The half-life drops by a factor of about 20. A few percent change in G (from a modest change in Q) can change lifetimes by orders of magnitude, explaining Geiger–Nuttall systematics [6, 1].

Problem 17.4 — Small Q/B limit for G

For $Z_1 = 90$, $Z_2 = 2$, $Q = 5.0\,\mathrm{MeV}$, and barrier height $B = 25\,\mathrm{MeV}$, evaluate the approximate Gamow factor $G \approx \pi Z_1 Z_2 e^2/(4\pi\varepsilon_0 \hbar v)$ with $v = \sqrt{2Q/\mu}$ and $\mu \approx 4\,\mathrm{u}$.

Solution 17.4

Step 1 (μ in SI-consistent units). Use $\mu c^2 \approx 3727\,\mathrm{MeV}$ (since $\mu \approx 4\,\mathrm{u}$).

Step 2 (speed).

$$v = c\sqrt{\frac{2Q}{\mu c^2}} = c\sqrt{\frac{10}{3727}} = 0.052c \approx 1.56 \times 10^{7}\,\mathrm{m/s}.$$

Step 3 (G). Using $\hbar c = 197\,\text{MeV fm}$ and $Z_1 Z_2 e^2/(4\pi\varepsilon_0) = 259.2\,\text{MeV fm}$:

$$G \approx \frac{\pi \times 259.2}{197 \times (v/c)} = \frac{\pi \times 259.2}{197 \times 0.0518} \approx 79.8.$$

Thus the leading small-Q/B estimate gives $P \approx e^{-2G} = e^{-159.6} \approx 5 \times 10^{-70}$.

Step 4 (finite-radius check). Here $Q/B = 0.20$, so the exact bracket in Eq. (1.30) is

$$\arccos\sqrt{0.20} - \sqrt{0.20(0.80)} = 0.707.$$

The exact finite-radius result is

$$G_{\text{exact}} = \frac{259.2}{197}\sqrt{\frac{2(3727)}{5.0}}\,(0.707) \approx 35.9, \qquad P_{\text{exact}} \approx e^{-71.8} \approx 7 \times 10^{-32}.$$

The leading value $G \approx 79.8$ deliberately drops the surface correction $-2\sqrt{Q/B}$; at $Q/B = 0.20$ that correction is not small numerically. Both results show the exponential suppression, while the comparison demonstrates why quantitative half-lives require the finite nuclear radius [6, 14].

Problem 17.5 — Selection rules for ^{243}Am

The parent ^{243}Am has $J^\pi = \frac{5}{2}^-$. For daughter ^{239}Np levels with $J^\pi = \frac{5}{2}^+$ (gs), $\frac{7}{2}^+$, and $\frac{5}{2}^-$ (75 keV), list the lowest allowed ℓ for each and predict which branch dominates.

Solution 17.5

Step 1 (parity rule). $\pi_i = \pi_f(-1)^\ell$. With $\pi_i = -$:

- $\frac{5}{2}^+$: need $(-1)^\ell = -1$, so ℓ odd. Lowest: $\ell = 1$.
- $\frac{7}{2}^+$: parity changes, so ℓ is odd. Angular coupling $|5/2 - 7/2| \le \ell \le 5/2 + 7/2$ gives $\ell \ge 1$; hence the lowest value is $\ell = 1$.
- $\frac{5}{2}^-$: parity match, ℓ even. $|5/2 - 5/2| = 0$, so $\ell = 0$ is allowed.

Step 2 (dominant branch). The $\ell = 0$ branch to $\frac{5}{2}^-$ at 74.660 keV has the thinnest barrier despite the reduced Q_i. DDEP gives 86.74(5)% intensity to this state versus 0.240(3)% to the ground state [20, 21, 28, 6].

Problem 17.6 — Assault frequency estimate

For $Q = 5\,\text{MeV}$, $V_0 = 35\,\text{MeV}$, $R = 7.5\,\text{fm}$, and $\mu \approx 4\,\text{u}$, estimate the assault frequency $f = v_0/(2R)$.

Solution 17.6

Step 1 (interior speed).

$$v_0 = \sqrt{\frac{2(Q + V_0)}{\mu}} = \sqrt{\frac{2 \times 40\,\text{MeV}}{\mu}}.$$

With $\mu c^2 \approx 3727\,\text{MeV}$:

$$v_0 = c\sqrt{\frac{80}{3727}} \approx 0.147c \approx 4.4 \times 10^7\ \text{m/s}.$$

Step 2 (frequency).

$$f = \frac{v_0}{2R} = \frac{4.4 \times 10^7\ \text{m/s}}{2 \times 7.5 \times 10^{-15}\ \text{m}} = 2.9 \times 10^{21}\ \text{s}^{-1}.$$

Step 3 (interpretation). The α presents itself at the barrier $\sim 10^{21}$ times per second, but escapes only with probability $P = e^{-2G} \ll 1$, yielding a much smaller $\lambda = S_\alpha f P$ [6, 1].

Bibliography

[1] R. A. Dunlap, *An Introduction to the Physics of Nuclei and Particles* (2nd ed.), IOP Publishing, Bristol (2023), DOI: 10.1088/978-0-7503-6094-4, Ch. 3 (Nuclear composition and size).

[2] W. Demtröder, *Nuclear and Particle Physics*, Undergraduate Lecture Notes in Physics, Springer, Cham (2023).

[3] S. Petrera, *Problems and Solutions in Nuclear and Particle Physics*, UNITEXT for Physics, Springer, Cham (2019).

[4] F. Terranova, *A Modern Primer in Particle and Nuclear Physics*, Oxford University Press (2021).

[5] S. D'Auria, *Introduction to Nuclear and Particle Physics*, Undergraduate Lecture Notes in Physics, Springer, Cham (2018).

[6] K. S. Krane, *Introductory Nuclear Physics*, Wiley, New York (1988).

[7] R. Hofstadter, "Electron scattering and nuclear structure," Rev. Mod. Phys. **28**, 214 (1956).

[8] H. F. Ehrenberg, R. Hofstadter, U. Meyer-Berkhout, D. G. Ravenhall, and S. E. Sobottka, "High-Energy Electron Scattering and the Charge Distribution of Carbon-12 and Oxygen-16," Phys. Rev. **113**, 666 (1959).

[9] H. Yukawa, "On the interaction of elementary particles. I," Proc. Phys.-Math. Soc. Japan **17**, 48 (1935).

[10] R. D. Woods and D. S. Saxon, "Diffuse surface optical model for nucleon-nuclei scattering," Phys. Rev. **95**, 577 (1954).

[11] H. G. J. Moseley, "The high-frequency spectra of the elements," Phil. Mag. **26**, 1024 (1913); **27**, 703 (1914).

[12] C. F. von Weizsäcker, "Zur Theorie der Kernmassen," Z. Phys. **96**, 431 (1935).

[13] P. Cappellaro, *Introduction to Applied Nuclear Physics* (MIT OpenCourseWare / LibreTexts), CC BY-NC-SA 4.0.

[14] J.-L. Basdevant, J. Rich, and M. Spiro, *Fundamentals in Nuclear Physics: From Nuclear Structure to Cosmology*, Springer, New York (2005).

[15] D. Tong, *Particle Physics*, Lecture notes (University of Cambridge / CERN school notes).

[16] M. G. Mayer, "On closed shells in nuclei. II," Phys. Rev. **75**, 1969 (1949).

[17] O. Haxel, J. H. D. Jensen, and H. E. Suess, "On the "magic numbers" in nuclear structure," Phys. Rev. **75**, 1766 (1949).

[18] T. Schmidt, "Über die magnetischen Momente der Atomkerne," Z. Phys. **106**, 358 (1937).

[19] L. W. Nordheim, "On spins, moments, and shells in nuclei," Phys. Rev. **78**, 294 (1950).

[20] Evaluated Nuclear Structure Data File (ENSDF), National Nuclear Data Center, Brookhaven National Laboratory, `https://www.nndc.bnl.gov/ensdf/`.

[21] NuDat 3, National Nuclear Data Center, Brookhaven National Laboratory, `https://www.nndc.bnl.gov/nudat3/`.

[22] N. J. Stone, "Table of nuclear magnetic dipole and electric quadrupole moments," At. Data Nucl. Data Tables **90**, 75 (2005); updated compilations at NNDC.

[23] W. N. Cottingham and D. A. Greenwood, *An Introduction to Nuclear Physics* (2nd ed.), Cambridge University Press, Cambridge (2001).

[24] H. Geiger and J. M. Nuttall, "The ranges of the α particles from the radioactive substances," Phil. Mag. **22**, 613 (1911).

[25] G. Gamow, "Zur Quantentheorie des Atomkernes," Z. Phys. **51**, 204 (1928).

[26] R. W. Gurney and E. U. Condon, "Wave mechanics and radioactive disintegration," Nature **122**, 439 (1928); Phys. Rev. **33**, 127 (1929).

[27] M. Wang, W. J. Huang, F. G. Kondev, G. Audi, and S. Naimi, "The AME 2020 atomic mass evaluation (II). Tables, graphs and references," Chin. Phys. C **45**, 030003 (2021).

[28] Laboratoire National Henri Becquerel (LNHB), Recommended decay data, `http://www.lnhb.fr/nuclear-data/nuclear-data-table/`.

[29] L. M. Langer, R. D. Moffat, and H. C. Price, Jr., "Low energy beta-ray spectra: P^{32} and Cu^{64}," Phys. Rev. **76**, 1725 (1949).

[30] L. M. Langer and H. C. Price, Jr., "Shapes of the beta-spectra of the forbidden transitions of Sb^{124}, Rb^{86}, Sr^{89}, Y^{91}, and Cs^{137}," Phys. Rev. **75**, 1769 (1949).

[31] D. C. Camp and L. M. Langer, "The shape of the ^{66}Ga positron spectrum and the contribution from $0^+ \to 0^+$ transitions," Phys. Rev. **129**, 1782 (1963).

[32] H. C. Verma, *Nuclear Physics: Fundamentals and Applications*, NPTEL/IIT Kanpur lecture series, `https://hcverma.in/ncl_phy_lectures`.

[33] International Atomic Energy Agency, *LiveChart of Nuclides*, evaluated structure, decay, reaction, and fission-yield data, `https://www-nds.iaea.org/relnsd/vcharthtml/VChartHTML.html`.

[34] T. Kibédi, T. W. Burrows, M. B. Trzhaskovskaya, P. M. Davidson, and C. W. Nestor, Jr., "Evaluation of theoretical conversion coefficients using BrIcc," Nucl. Instrum. Methods Phys. Res. A **589**, 202 (2008), DOI: 10.1016/j.nima.2008.02.051.

[35] D. A. Brown *et al.*, "ENDF/B-VIII.0: The 8th major release of the nuclear reaction data library with CIELO-project cross sections, new standards and thermal scattering data," Nucl. Data Sheets **148**, 1 (2018), DOI: 10.1016/j.nds.2018.02.001.

[36] B. Acharya *et al.*, "Solar fusion III: New data and theory for hydrogen-burning stars," Rev. Mod. Phys. **97**, 035002 (2025), DOI: 10.1103/8lm7-gs18.

[37] S. N. Ghoshal, "An experimental verification of the theory of compound nucleus," Phys. Rev. **80**, 939 (1950), DOI: 10.1103/PhysRev.80.939.

[38] D. Adhikari *et al.* (PREX Collaboration), "Accurate determination of the neutron skin thickness of ^{208}Pb through parity-violation in electron scattering," Phys. Rev. Lett. **126**, 172502 (2021), DOI: 10.1103/PhysRevLett.126.172502.

[39] B. T. Reed, F. J. Fattoyev, C. J. Horowitz, and J. Piekarewicz, "Implications of PREX-II on the equation of state of neutron-rich matter," Phys. Rev. Lett. **126**, 172503 (2021), DOI: 10.1103/PhysRevLett.126.172503.

[40] B. Hu *et al.*, "Ab initio predictions link the neutron skin of ^{208}Pb to nuclear forces," Nature Phys. **18**, 1196 (2022), DOI: 10.1038/s41567-022-01715-8.

[41] E. Epelbaum, H.-W. Hammer, and U.-G. Meißner, "Modern theory of nuclear forces," Rev. Mod. Phys. **81**, 1773 (2009), DOI: 10.1103/RevModPhys.81.1773.

[42] H.-W. Hammer, S. König, and U. van Kolck, "Nuclear effective field theory: Status and perspectives," Rev. Mod. Phys. **92**, 025004 (2020), DOI: 10.1103/RevModPhys.92.025004.

[43] T. Otsuka, A. Gade, O. Sorlin, T. Suzuki, and Y. Utsuno, "Evolution of shell structure in exotic nuclei," Rev. Mod. Phys. **92**, 015002 (2020), DOI: 10.1103/RevModPhys.92.015002.

[44] H. Hergert, S. K. Bogner, T. D. Morris, A. Schwenk, and K. Tsukiyama, "The in-medium similarity renormalization group: A novel ab initio method for nuclei," Phys. Rep. **621**, 165 (2016), DOI: 10.1016/j.physrep.2015.12.007.

[45] J. M. Lattimer and M. Prakash, "The equation of state of hot, dense matter and neutron stars," Phys. Rep. **621**, 127 (2016), DOI: 10.1016/j.physrep.2015.12.005.

[46] J. M. Lattimer, "Neutron stars and the nuclear matter equation of state," Annu. Rev. Nucl. Part. Sci. **71**, 433 (2021), DOI: 10.1146/annurev-nucl-102419-124827.

[47] B. P. Abbott *et al.* (LIGO Scientific Collaboration and Virgo Collaboration), "GW170817: Observation of gravitational waves from a binary neutron star inspiral," Phys. Rev. Lett. **119**, 161101 (2017), DOI: 10.1103/PhysRevLett.119.161101.

[48] M. J. Dolinski, A. W. P. Poon, and W. Rodejohann, "Neutrinoless double-beta decay: Status and prospects," Annu. Rev. Nucl. Part. Sci. **69**, 219 (2019), DOI: 10.1146/annurev-nucl-101918-023407.

[49] M. Agostini, G. Benato, J. A. Detwiler, J. Menéndez, and F. Vissani, "Toward the discovery of matter creation with neutrinoless $\beta\beta$ decay," Rev. Mod. Phys. **95**, 025002 (2023), DOI: 10.1103/RevModPhys.95.025002.

[50] P. Gysbers *et al.*, "Discrepancy between experimental and theoretical β-decay rates resolved from first principles," Nature Phys. **15**, 428 (2019), DOI: 10.1038/s41567-019-0450-7.

[51] H. L. Crawford, K. Fossez, S. König, and A. Spyrou, "A vision for the science of rare isotopes," Annu. Rev. Nucl. Part. Sci. **74**, 141 (2024), DOI: 10.1146/annurev-nucl-121423-091501.

[52] Nuclear Science Advisory Committee, *A New Era of Discovery: The 2023 Long Range Plan for Nuclear Science*, U.S. Department of Energy and National Science Foundation (2023), `https://nuclearsciencefuture.org/`.

[53] S. A. Giuliani, Z. Matheson, W. Nazarewicz, E. Olsen, P.-G. Reinhard, J. Sadhukhan, B. Schuetrumpf, N. Schunck, and P. Schwerdtfeger, "Colloquium: Superheavy elements: Oganesson and beyond," Rev. Mod. Phys. **91**, 011001 (2019), DOI: 10.1103/RevModPhys.91.011001.

[54] N. Schunck and D. Regnier, "Theory of nuclear fission," Prog. Part. Nucl. Phys. **125**, 103963 (2022), DOI: 10.1016/j.ppnp.2022.103963.

[55] I. Counts, J. Hur, D. P. L. Aude Craik, H. Jeon, C. Leung, J. C. Berengut, A. Geddes, A. Kawasaki, W. Jhe, and V. Vuletić, "Evidence for nonlinear isotope shift in Yb^+ search for new boson," Phys. Rev. Lett. **125**, 123002 (2020), DOI: 10.1103/PhysRevLett.125.123002.

[56] I. Angeli and K. P. Marinova, "Table of experimental nuclear ground state charge radii: An update," At. Data Nucl. Data Tables **99**, 69 (2013), DOI: 10.1016/j.adt.2011.12.006.

[57] S. Kraemer *et al.*, "Observation of the radiative decay of the ^{229}Th nuclear clock isomer," Nature **617**, 706 (2023), DOI: 10.1038/s41586-023-05894-z.